

Numerical analysis of motional mode coupling of sympathetically cooled two-ion crystals

Li-Jun Du(杜丽军), Yan-Song Meng(蒙艳松), Yu-Ling He(贺玉玲), and Jun Xie(谢军)
Citation: Chin. Phys. B, 2021, 30 (**7**): 073702. DOI: 10.1088/1674-1056/abfc3e
Journal homepage: http://cpb.iphy.ac.cn; http://iopscience.iop.org/cpb

What follows is a list of articles you may be interested in

Setup of a dipole trap for all-optical trapping

Miao Wang(王淼), Zheng Chen(陈正), Yao Huang(黄垚), Hua Guan(管桦), and Ke-Lin Gao(高克林)
Chin. Phys. B, 2021, 30 (**5**): 053702. DOI: 10.1088/1674-1056/abd767

Optimization of endcap trap for single-ion manipulation

Yuan Qian(钱源), Chang-Da-Ren Fang(方长达人), Yao Huang(黄垚), Hua Guan(管桦), Ke-Lin Gao(高克林)
Chin. Phys. B, 2018, 27 (**6**): 063701. DOI: 10.1088/1674-1056/27/6/063701

Quantitative evaluation of space charge effects of laser-cooled three-dimensional ion system on a secular motion period scale

Li-Jun Du(杜丽军), Hong-Fang Song(宋红芳), Shao-Long Chen(陈邵龙), Yao Huang(黄垚), Xin Tong(童昕), Hua Guan(管桦), Ke-Lin Gao(高克林)
Chin. Phys. B, 2018, 27 (**4**): 043701. DOI: 10.1088/1674-1056/27/4/043701

An optimized ion trap geometry to measure quadrupole shifts of ^{171}Yb+ clocks

N Batra, B K Sahoo, S De
Chin. Phys. B, 2016, 25 (**11**): 113703. DOI: 10.1088/1674-1056/25/11/113703

Compensating for excess micromotion of ion crystals

Du Li-Jun, Chen Ting, Song Hong-Fang, Chen Shao-Long, Li Hai-Xia, Huang Yao, Tong Xin, Guan Hua, Gao Ke-Lin
Chin. Phys. B, 2015, 24 (**8**): 083702. DOI: 10.1088/1674-1056/24/8/083702

Numerical analysis of motional mode coupling of sympathetically cooled two-ion crystals*

Li-Jun Du(杜丽军)[1,2], Yan-Song Meng(蒙艳松)[1,2,†], Yu-Ling He(贺玉玲)[1,2], and Jun Xie(谢军)[2,3]

[1] China Academy of Space Technology (Xi'an), Xi'an 710100, China
[2] National Key Laboratory of Science and Technology on Space Microwave, China Academy of Space Technology (Xi'an), Xi'an 710100, China
[3] China Academy of Space Technology, Beijing 100094, China

(Received 3 January 2021; revised manuscript received 21 March 2021; accepted manuscript online 28 April 2021)

A two-ion pair in a linear Paul trap is extensively used in the research of the simplest quantum-logic system; however, there are few quantitative and comprehensive studies on the motional mode coupling of two-ion systems yet. This study proposes a method to investigate the motional mode coupling of sympathetically cooled two-ion crystals by quantifying three-dimensional (3D) secular spectra of trapped ions using molecular dynamics simulations. The 3D resonance peaks of the $^{40}Ca^{+}$–$^{27}Al^{+}$ pair obtained by using this method were in good agreement with the 3D in- and out-of-phase modes predicted by the mode coupling theory for two ions in equilibrium and the frequency matching errors were lower than 2%. The obtained and predicted amplitudes of these modes were also qualitatively similar. It was observed that the strength of the sympathetic interaction of the $^{40}Ca^{+}$–$^{27}Al^{+}$ pair was primarily determined by its axial in-phase coupling. In addition, the frequencies and amplitudes of the ion pair's resonance modes (in all dimensions) were sensitive to the relative masses of the ion pair, and a decrease in the mass mismatch enhanced the sympathetic cooling rates. The sympathetic interactions of the $^{40}Ca^{+}$–$^{27}Al^{+}$ pair were slightly weaker than those of the $^{24}Mg^{+}$–$^{27}Al^{+}$ pair, but significantly stronger than those of $^{9}Be^{+}$–$^{27}Al^{+}$. However, the Doppler cooling limit temperature of $^{40}Ca^{+}$ is comparable to that of $^{9}Be^{+}$ but lower than approximately half of that of $^{24}Mg^{+}$. Furthermore, laser cooling systems for $^{40}Ca^{+}$ are more reliable than those for $^{24}Mg^{+}$ and $^{9}Be^{+}$. Therefore, $^{40}Ca^{+}$ is probably the best laser-cooled ion for sympathetic cooling and quantum-logic operations of $^{27}Al^{+}$ and has particularly more notable comprehensive advantages in the development of high reliability, compact, and transportable $^{27}Al^{+}$ optical clocks. This methodology may be extended to multi-ion systems, and it will greatly aid efforts to control the dynamic behaviors of sympathetic cooling as well as the development of low-heating-rate quantum logic clocks.

Keywords: sympathetic cooling, coupled oscillations, secular motion, radio-frequency ion traps

PACS: 37.10.Ty, 37.10.Rs, 37.90.+j, 31.15.xv **DOI:** 10.1088/1674-1056/abfc3e

1. Introduction

An important tool in the study of objective reality is the precise control and measurement of neutral, charged atomic and molecular quantum states because they play an important role in the discovery of new physical phenomena and in the testing of the fundamental laws of physics.[1] Through the use of the laser cooling and atom (ion) trapping techniques, the transition frequency of atomic and molecular systems can be controlled to a precision of 10^{-19},[2] which is the highest level of precision among all precision measurement techniques. The preparation and measurement of cold ion systems is typically performed using a red-detuned laser, which interacts with a closed cycling transition of the target ion to dissipate its kinetic energy and suppress the Doppler effect. This ensures that the quantum states of the ions are coherent and ready for precision measurements. However, many candidate ions that may be used for the development of precise frequency standards or probing the time variations of the fine structure constant[3–7] are difficult to cool, owing to the lack of cycling transitions or suitable lasers. This makes precise measurements of their transition lines impossible. Therefore, a generally applicable method for the preparation of cold ions that does not require direct laser cooling while efficiently suppressing quantum decoherence in ion systems is crucial for ion-based precision measurements and applications.

The Wineland group in the National Institute of Standards and Technology constructed the optical measurement systems for $^{27}Al^{+}$, which are based on sympathetic cooling using $^{9}Be^{+}$ and $^{24}Mg^{+}$.[2,8,9] These "logic" ions also enable the internal quantum transitions of $^{27}Al^{+}$ to be measured via their external degrees of freedom. This method was used to create frequency standards with an accuracy of 10^{-19}, which were then used to validate special and general relativity.[2,8] Sympathetic cooling and quantum-logic measurements of an ion are performed by trapping a laser-cooled ion (LCI) and a sympathetically cooled ion (SCI) in a radio-frequency (RF) ion trap. These ion species will then be tightly coupled to each other through Coulomb interactions. Subsequently, a resonant energy transfer occurs between the SCI and the colder LCI, while heat is continuously removed from the system through laser Doppler cooling

*Project supported by the National Natural Science Foundation of China (Grant No. 11803023), the Equipment Pre-research Foundation (Grant No. 6142411196406), and Key Research and Development Program of Shaanxi Province, China (Grant No. 2017ZDXM-GY-113).

†Corresponding author. E-mail: yansmeng@163.com

© 2021 Chinese Physical Society and IOP Publishing Ltd

and sideband cooling. This continues until the two-ion system is cooled to thermal equilibrium by motional mode coupling (or even to the quantum mechanical ground state[9] in some cases). Once this state is achieved, the internal quantum state of the SCI and the external vibrational quantum state of the coupled SCI-LCI system can be manipulated using suitable pulsed lasers, thereby influencing the internal quantum state of the LCI. Quantum-logic operations on the SCI's internal quantum state may then be performed by probing the internal quantum state of the LCI. Over the past 20 years, sympathetic cooling has been used in trapped ion systems to cool a variety of systems, both small (electrons) and large (biological molecules), to mK or μK levels.[10,11] It is now possible to control the motional modes and coupling characteristics of sympathetically cooled two-ion systems to hitherto unachievable levels of precision. This breakthrough enables precise quantum manipulations and measurements of charged ion systems with remarkable physical properties, which typically could not be directly laser-cooled. This allowed further precision in atomic clocks and in testing the fundamental theories of physics as well as in the construction of scalable quantum computers. Sympathetic cooling and quantum-logic operations based on ion trapping are now an important area of research for quantum logic clocks, quantum information processing, quantum computing, and cold chemistry.[12–17] Motional mode coupling between the SCI and LCI is an important factor for sympathetic cooling efficiency. It is also necessary for quantum-logic detection because it links the internal quantum states of the LCI and SCI. Therefore, the precise assessment and control of the motional mode coupling between the LCI and SCI are crucial for sympathetic ion cooling and high-precision ion spectroscopy.

In terms of structure and coupling mechanism, a linear two-ion pair in a linear Paul trap is the simplest quantum-logic system, and it has been widely implemented in scientific studies.[18] However, systematic studies on the motional mode coupling of two-ion systems are scarce, and the optimization of LCI–SCI interactions, mixed-ion systems, and potential fields remains poorly explored. Furthermore, the factors that influence the resonance modes and energy transfers of LCI–SCI systems have not been quantified. Owing to its physical properties, $^{27}Al^{+}$ is one of the best candidate ions for atomic clocks and precision measurements, and it has been extensively studied.[2,8,9] However, direct laser cooling of $^{27}Al^{+}$ is still very difficult, owing to the limitations of deep ultraviolet laser technology.[19] In this study, we will use the sympathetic cooling and quantum-logic operations of $^{27}Al^{+}$ to study the motional mode coupling of LCI–SCI ion pairs.

2. Linear Paul trap for sympathetic cooling of ion pairs and its equivalent resonance model

The linear Paul trap and the corresponding coordinates used in our study are shown in Fig. 1. The lengths of the trapping part (B) and the remaining parts (A,C) of each electrode are $2z_0 = 5.90$ mm and $2z_e = 24.00$ mm, respectively. The diameter of each electrode rod is $d = 8.00$ mm, and the minimum distances between the trap axis and all electrodes are $r_0 = 3.50$ mm. The confinement of the ions in the radial plane is obtained by applying a pair of RF fields ($\pm 1/2U_{rf}\cos(\Omega_{rf}t)$) with the same frequency and amplitude and a phase difference of π to two pairs of diagonal electrode rods ($A_{1,3}$, $B_{1,3}$, $C_{1,3}$, and $A_{2,4}$, $B_{2,4}$, $C_{2,4}$). The confinement of the ions in the axial direction is obtained by applying direct current (DC) voltage U_{end} to the ends of the electrodes (A and C). A detailed description of the linear Paul trap can be found in Refs. [20,21]. After the two-ion system is sympathetically cooled to the crystalline state, the equilibrium distance between the two ions becomes $z = (Qz_0^2/(32U_{end}\pi\varepsilon_0))^{1/3}$,[22] where Q is the electron charge of each ion, and ε_0 is the permittivity of free space. These ions exhibit three-dimensional (3D) resonant motions about their equilibrium positions, which are coupled to each other to an extent. If we do not consider high-order resonances,[23] the motional mode couplings of the two-ion system divide vibrational modes into the in- and out-of-phase eigenmodes. The external motional states may be expressed as the following Hamiltonian:

$$\hat{H} = \hbar\omega_i\left(\hat{a}_i^{\dagger}\hat{a}_i + \frac{1}{2}\right) + \hbar\omega_o\left(\hat{a}_o^{\dagger}\hat{a}_o + \frac{1}{2}\right), \tag{1}$$

where $\hat{a}_i^{\dagger}$, $\hat{a}_i$, $\hat{a}_o^{\dagger}$, and $\hat{a}_o$ are the standard harmonic oscillator ladder operators of the in- and out-of-phase vibrational modes, respectively. The coupled vibrational displacements of the LCI and SCI are $\boldsymbol{l}_{SCI}$ and $\boldsymbol{l}_{LCI}$, respectively:[24,25]

$$\boldsymbol{l}_{SCI} \approx z_i b_1 \sin(\omega_i t + \phi_i) + z_o b_2 \cos(\omega_o t + \phi_o), \tag{2}$$

$$\boldsymbol{l}_{LCI} \approx \frac{z_i b_2}{\sqrt{\mu}}\sin(\omega_i t + \phi_i) - \frac{z_o b_1}{\sqrt{\mu}}\cos(\omega_o t + \phi_o). \tag{3}$$

In these equations, ω_i and ω_o are the angular eigenfrequencies of the in- and out-of-phase modes, respectively, and ϕ_i and ϕ_o are their phases. z_i and z_o are the modal amplitudes of the ion in- and out-of-phase vibrations, respectively. The mass ratio of the singly charged ion pair is $\mu = m_{LCI}/m_{SCI}$. b_1 and b_2 are the components of the normalized eigenvector of the in-phase mode, which satisfy $b_1^2 + b_2^2 = 1$ in each dimension. The normalized eigenvector ($b_{1,z}$ and $b_{2,z}$) of the axial vibrational modes of the ions depends directly on the mass ratios μ of the ion pair and satisfies

$$b_{1,z} = \sqrt{\frac{1-\mu}{2\sqrt{1-\mu+\mu^2}} + \frac{1}{2}}. \tag{4}$$

The normalized eigenvector ($b_{1,r}$ and $b_{2,r}$) of the radial vibrational modes depends on both the mass ratios μ of the ion pair and the radial-to-axial secular frequency ratio of the SCI, $\eta = \omega_{SCI\text{-}r}/\omega_{SCI\text{-}z}$, approximated by a harmonic pseudopotential model[25] and satisfies

$$b_{1,r} = \sqrt{\frac{\mu - \mu^2 + \eta^2(\mu^2-1)}{2\sqrt{\eta^4(\mu^2-1)^2 - 2\eta^2(\mu-1)^2\mu(\mu+1) + \mu^2(1-\mu+\mu^2)}} + \frac{1}{2}}. \tag{5}$$

The coupling intensities of the in- and out-of-phase vibrational modes of a LCI–SCI heteronuclear ion pair in specific dimensions are characterized by the absolute amplitude ratio of the heteronuclear ion pair in these modes[26]

$$I_{\text{in}} = \text{A}(\text{SCI}_{\text{in}})/\text{A}(\text{LCI}_{\text{in}}) = b_{1z,r} \times \sqrt{\mu}/b_{2z,r}, \tag{6}$$

$$I_{\text{out}} = \text{A}(\text{SCI}_{\text{out}})/\text{A}(\text{LCI}_{\text{out}}) = b_{2z,r} \times \sqrt{\mu}/b_{1z,r}. \tag{7}$$

The closer I_{in} and I_{out} are to 1, the stronger the coupling is.

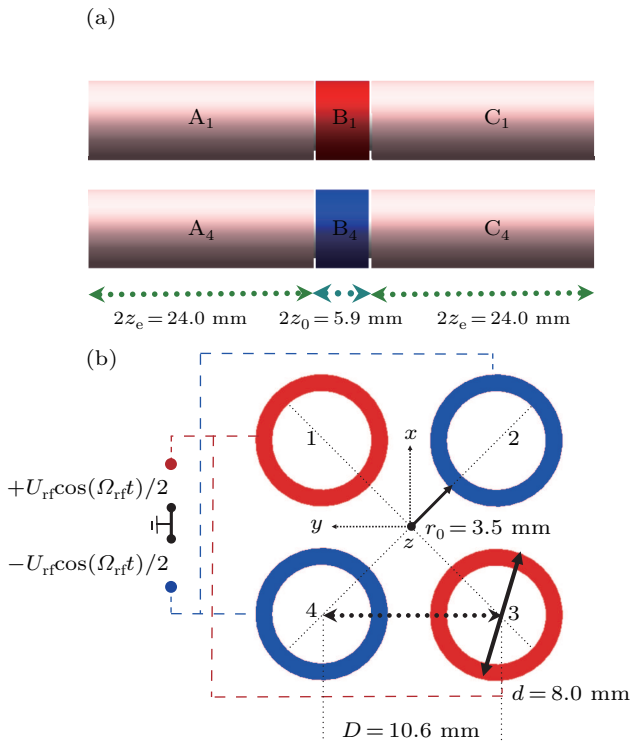


Fig. 1. Schematic of the (a) linear Paul trap and (b) RF potential.

3. Secular spectra of sympathetically cooled ion pairs

The dynamics of RF-trapped ion systems can be approximated by using a harmonic pseudo potential model. Secular spectra are effective means for probing the dynamics of ion coupling, and they are also important for understanding and controlling sympathetic cooling and quantum-logic detection processes. We have used molecular dynamics simulations to study the dynamic coupling characteristics, spatial configuration, sympathetic cooling mechanism, and efficiency effect of ion pairs. The "leap frog" algorithm[27–29] is applied to solve the equation of motion of each particle. The kinematics information is monitored while the cloud moves under the influence of the RF trapping field, the Coulomb interaction forces, random collision force, and laser light interaction force. A detailed description of the numerical simulation methods can be found in Ref. [21]. The secular spectra of SCI pairs are obtained by applying a fast Fourier transform to the 3D coordinates of ions at different time.

3.1. Motional resonance spectrum of a single ion

The axial motions of a linearly trapped ion are determined by using the axial electrostatic potential. By minimizing the radial micromotions of the ion using the fluorescence modulation technique,[30] the radial (x and y) forces and secular motions of the ion system converge to a set point, and its motions are then jointly determined by the RF potential and axial electrostatic potential. Figure 2 shows the 3D secular spectra of singly trapped single $^{40}Ca^+$ and $^{27}Al^+$ ions under the same RF field ($\Omega_{\text{rf}} = 3.7148$ MHz, $U_{\text{rf1}} = 200$ V, $U_{\text{end}} = 3.5$ V), and the $^{27}Al^+$ spectra were obtained by removing the $^{40}Ca^+$ contribution to the $^{40}Ca^+$–$^{27}Al^+$ pair through secular motional excitation or by controlling a radially symmetric electrostatic potential. Because the radial trapping strength of the trapping potential is higher than the axial trapping strength for a given ion, the radial secular frequency is higher than the axial secular frequency.

The axial and radial motional resonances of single $^{40}Ca^+$ and $^{27}Al^+$ ions are primarily basic modes. Their axial peaks are $\omega_{\text{Al-}z} = 137.315$ kHz and $\omega_{\text{Ca-}z} = 112.658$ kHz, and their radial peaks are $\omega_{\text{Al-}r} = 268.254$ kHz and $\omega_{\text{Ca-}r} = 174.301$ kHz, respectively. In the harmonic pseudo potential model, the axial and radial secular frequencies of $^{40}Ca^+$ and $^{27}Al^+$ satisfy[24]

$$\omega_{\text{Al-}z}/\omega_{\text{Ca-}z} = \sqrt{\frac{M_{^{40}\text{Ca}^+}}{M_{^{27}\text{Al}^+}}}, \tag{8}$$

$$\omega_{\text{Al-}r}/\omega_{\text{Ca-}r} = \frac{M_{^{40}\text{Ca}^+}}{M_{^{27}\text{Al}^+}} \sqrt{\frac{1+\frac{1}{2}\beta^2_{^{40}\text{Ca}^+}}{1+\frac{1}{2}\beta^2_{^{27}\text{Al}^+}}}. \tag{9}$$

In these equations, $\beta = \omega_z/\omega_r$ is the ratio between the axial and radial equivalent binding strength of an ion.[24] The matching errors between the axial and radial resonance frequencies obtained from the simulations and their approximations from the equivalent pseudo potential were lower than 0.000168% and 0.509%, respectively (the accuracy of the latter was primarily limited by ignoring the high-order nonharmonic potential in the equivalent pseudo potential approximations). Thus, it is shown that the effect of high-order resonant modes on 3D resonance modes of single ions in a linear

trap is negligible. Therefore, these modes are well approximated by the harmonic pseudo potential model.

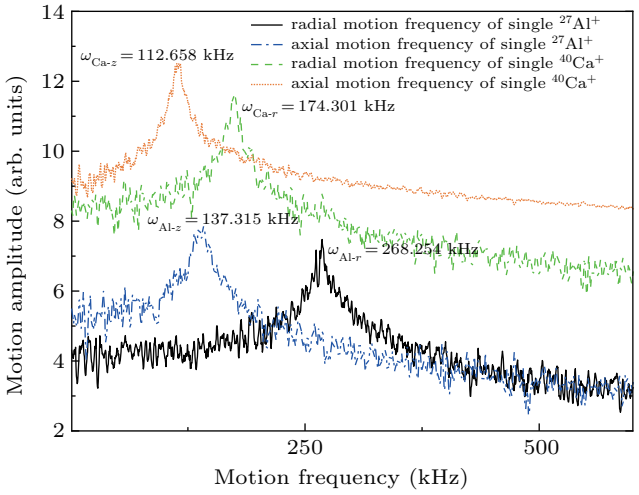


Fig. 2. 3D secular spectra of trapped single $^{40}Ca^+$ and $^{27}Al^+$ ions. The $^{27}Al^+$ spectra were obtained by removing the $^{40}Ca^+$ contribution to the $^{40}Ca^+$–$^{27}Al^+$ pair through secular motional excitation or by controlling the radially symmetric electrostatic potential.

3.2. Motional mode coupling in the $^{40}Ca^+$–$^{27}Al^+$ pair

Sympathetic cooling of a single $^{27}Al^+$ ion by a single $^{40}Ca^+$ ion leads to the formation of a $^{40}Ca^+$–$^{27}Al^+$ crystal. Long-range Coulomb interactions will then cause their simple harmonic motions to couple and establish new normal modes of motion. The 3D secular spectra of this two-ion system (under the RF field: $\Omega_{rf} = 3.7148$ MHz, $U_{rf1} = 200$ V, $U_{end} = 3.5$ V) are shown in Fig. 3. In the axial motional spectrum (Fig. 3(a)), $^{40}Ca^+$ and $^{27}Al^+$ both exhibit three sets of resonances at ω_{1z} ($\omega_{Al\text{-}z} \approx \omega_{Ca\text{-}z} = 124.561$ kHz), ω_{2z} ($\omega_{Al\text{-}z} = 218.089$ kHz, $\omega_{Ca\text{-}z} = 220.639$ kHz, and $\omega_{Ca\text{-}z}/\omega_{Al\text{-}z} = 1.012$), and ω_{3z} ($\omega_{Al\text{-}z} = 296.737$ kHz, $\omega_{Ca\text{-}z} = 297.162$ kHz, and $\omega_{Ca\text{-}z}/\omega_{Al\text{-}z} = 1.001$). The one-to-one correspondence between the axial resonances of $^{40}Ca^+$ and $^{27}Al^+$ implies that their axial resonance modes are tightly coupled, which is beneficial for efficient energy transfer and sympathetic cooling. Based on the mode coupling theory for two ions in equilibrium,[25,26] the axial out-of-phase mode of the $^{40}Ca^+$–$^{27}Al^+$ pair should have a higher frequency than their in-phase mode. The frequencies of the in- and out-of-phase modes are $\omega_{i\text{-}z} = 122.173$ kHz and $\omega_{o\text{-}z} = 219.650$ kHz, respectively. The out-of-phase mode is dominated by the resonance intensity of the lighter $^{27}Al^+$ ion (the amplitude ratio of the out-of-phase mode is $A(Al_{out})/A(Ca_{out}) = b_{2,z} \times \sqrt{\mu}/b_{1,z} = 1.790$), and the in-phase mode is dominated by the resonance intensity of the heavier $^{40}Ca^+$ ion (the amplitude ratio of the in-phase mode is $A(Al_{in})/A(Ca_{in}) = b_{1,z} \times \sqrt{\mu}/b_{2,z} = 0.828$). The coupling intensity of the axial in-phase mode is stronger than that of the out-of-phase mode. In the secular spectrum of the $^{40}Ca^+$–$^{27}Al^+$ ion pair, the first and second sets of resonant frequencies, ω_{1z} and ω_{2z}, are the in- and out-of-phase modes, respectively, and the matching errors of these modes are 1.956% and 0.711%, respectively. Thus, it is shown that the relative intensities of the axial resonance peaks in Fig. 3(a) are generally in good agreement with the theoretically predicted relative mode amplitudes. The third set of resonant frequencies, ω_{3z}, corresponds to the high-order coupling between $^{40}Ca^+$ and $^{27}Al^+$. High-order coupling effects cannot be obtained analytically as yet. However, the secular spectrum shows that $^{40}Ca^+$ and $^{27}Al^+$ are still significantly coupled in the ω_{3z} frequency mode, which should be beneficial for sympathetic cooling.

In the radial secular spectrum of the $^{40}Ca^+$–$^{27}Al^+$ pair (Fig. 3(b)), both $^{40}Ca^+$ and $^{27}Al^+$ exhibit two sets of resonant frequencies, which are ω_{1r} ($\omega_{Al\text{-}r} = 148.369$ kHz and $\omega_{Ca\text{-}r} = 147.518$ kHz, which give $\omega_{Ca\text{-}r}/\omega_{Al\text{-}r} = 1.021$) and ω_{2r} ($\omega_{Al\text{-}r} = 253.800$ kHz and $\omega_{Ca\text{-}r} = 252.864$ kHz, which give $\omega_{Ca\text{-}r}/\omega_{Al\text{-}r} = 0.996$). Compared with $^{40}Ca^+$, the radial secular spectrum of $^{27}Al^+$ has two more high-frequency resonance modes: ω_{3r} ($\omega_{Al\text{-}r} = 367.308$ kHz) and ω_4 ($\omega_{Al\text{-}r} = 441.705$ kHz). Based on the mode coupling theory for two ions in equilibrium, the radial in-phase mode of the $^{40}Ca^+$–$^{27}Al^+$ pair should have a higher frequency than their out-of-phase mode. The frequencies of the in- and out-of-phase modes are $\omega_{i\text{-}r} = 253.071$ kHz and $\omega_{o\text{-}r} = 151.188$ kHz, respectively. The in- and out-of-phase modes are dominated by the resonance intensities of the lighter $^{27}Al^+$ and heavier $^{40}Ca^+$ ions, and their amplitude ratios are $A(Al_{in})/A(Ca_{in}) = b_{1,r} \times \sqrt{\mu}/b_{2,r} = 6.23294$ and $A(Al_{out})/A(Ca_{out}) = b_{2,r} \times \sqrt{\mu}/b_{1,r} = 0.23763$, respectively. The in- and out-of-phase modes of the ions are weakly coupled, and the coupling of the out-of-phase mode is slightly stronger than that of the in-phase mode. From the radial secular spectrum of the ion pair shown in Fig. 3(b), it may be deduced that ω_{1r} is the out-of-phase mode and ω_{2r} is the in-phase mode, and the matching errors of these modes are 1.864% and 0.2879%, respectively. Therefore, the relative intensities in the radial secular spectrum of the $^{27}Al^+$–$^{40}Ca^+$ pair are in agreement with the theoretically predicted relative mode amplitudes. In addition to in- and out-of-phase modes, the $^{27}Al^+$ spectrum also contains two significant high-frequency modes (ω_{3r} and ω_{4r}), which are higher-order couplings between $^{40}Ca^+$ and $^{27}Al^+$. ω_{3r} ($\omega_{Al\text{-}r} = 367.308$ kHz) represents the combined frequency effect of the axial out-of-phase mode ($\omega_{o\text{-}z} = 219.650$ kHz) and radial out-of-phase mode ($\omega_{o\text{-}r} = 151.188$ kHz) of the ion pair, and the matching error is less than 0.961%. A method to quantify the coupling of ω_{4r} is yet to be established. However, the secular spectra show that the ω_{3r} and ω_{4r} high-frequency modes of $^{27}Al^+$ do not couple with $^{40}Ca^+$, which indicates that their contribution to sympathetic cooling is negligible.

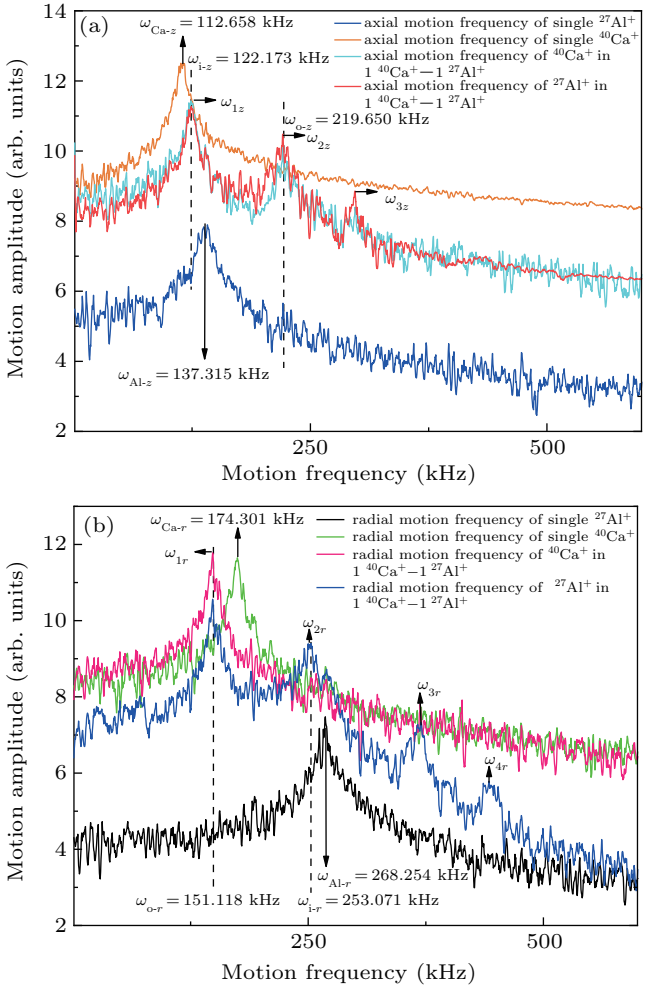


Fig. 3. (a) Axial and (b) radial secular spectra of the $^{40}Ca^+$–$^{27}Al^+$ two-ion crystal formed by the sympathetic cooling of a single $^{27}Al^+$ ion using a single $^{40}Ca^+$ ion.

Because the radial coupling modes of the $^{40}Ca^+$–$^{27}Al^+$ pair are both fewer in number and weaker than their axial coupling modes, the efficiency of sympathetic cooling in this system is primarily determined by the axial resonance coupling. It may also be observed that the 3D secular spectra of the $^{40}Ca^+$–$^{27}Al^+$ pair are generally in good agreement with the in- and out-of-phase modes predicted by the mode coupling theory for a pair of ions in equilibrium. The matching errors were primarily caused by the inability of mode coupling theory to account for higher-order coupling.

4. Effect of mass mismatches on the motional mode coupling of two ions and selection of an optimal LCI

Differences in the ion mass in a singly charged two-ion system will inevitably lead to differences in its effective potential and RF heating rates.[30] Quantitative studies on the effect of mass ratio variations on the motional mode coupling in two-ion systems are crucial to construct optimal ion systems for sympathetic cooling and high-fidelity quantum-logic operations. At present, laser cooling can only be used on ions with simple energy structures, such as $^{9}Be^+$, $^{24}Mg^+$, $^{40}Ca^+$, $^{87}Sr^+$, $^{113}Cd^+$, $^{137}Ba^+$, and $^{171}Yb^+$. Other ion systems either lack a closed cycling transition or have cycling transitions that cannot be pumped by existing lasers. Once the target SCI is identified, the selection of an optimal LCI is an important factor that affects the efficiency of sympathetic cooling and the fidelity of precision measurements.

4.1. Effect of mass mismatches on the motional mode coupling resonance frequencies

Because the in- and out-of-phase resonance modes are the lowest-order coupled modes of an ion pair in equilibrium, they are sensitive to the distribution of relative masses in the ion pair. Figure 4 illustrates the relationships between the predicted resonant-mode frequencies of an LCI–SCI pair and their mass ratio μ (the radial stability parameter of SCI is $q_{\rm SCI} = 0.215$, and the pseudo potential well depth of SCI is $D_{\rm r,SCI} = 0.136$ eV). The axial out-of-phase mode of the ion pair always has a higher frequency than the in-phase mode, and the minimum difference between these frequencies occurs at $\mu = 1$. At this point, the in-phase vibrational frequency is the axial secular frequency of the SCI, ω_z, and the frequency of the out-of-phase vibration is $\sqrt{3}\omega_z$. The difference in the frequencies between these modes increases with an increase in the mass difference. The frequency of the ion pair's radial in-phase mode is always higher than that of the out-of-phase mode. The frequency of the in-phase mode becomes more sensitive to mass mismatches when $\mu < 1$, and the frequency of out-of-phase mode becomes more sensitive to the mass mismatches when $\mu > 1$. If μ exceeds a particular threshold, the radial out-of-phase mode completely disappears. This threshold depends on the relative axial and radial binding strengths of the ions, and can be expressed as $\mu_{\rm T} = 4(1-\beta^2)/(4\beta^2 - 3\beta^4)$, which is based on the mode coupling theory for two ions in equilibrium,[25,26] and increasing the relative radial binding strength will increase the $\mu_{\rm T}$ threshold of the radial out-of-phase mode.

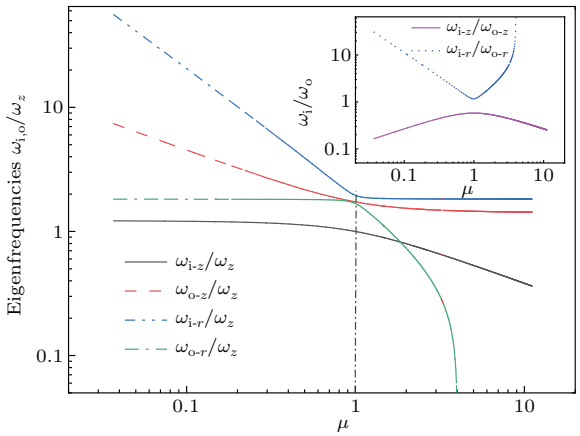


Fig. 4. Relationships between the resonant-mode frequencies of an LCI–SCI pair and their mass ratio μ.

4.2. Effect of mass mismatches on the motional mode coupling vibrational amplitudes

In an ion pair with resonating normal modes, the relative mode amplitudes significantly affect the mode coupling strength and the sympathetic cooling rates. Figure 5 illustrates the amplitude ratios of the in- and out-of-phase modes of an LCI–SCI pair in each dimension, which were simulated by using the mode coupling theory for a pair of ions in equilibrium (the radial stability parameter of SCI is $q_{\mathrm{SCI}} = 0.215$, and the pseudo potential well depth of SCI is $D_{\mathrm{r,SCI}} = 0.136$ eV).[25] The strength of the external-state coupling in any mode increases as the ion mode amplitudes become more similar, which effectively increases the rates of sympathetic cooling. It is possible to maximize the sympathetic cooling efficiency by selecting a suitable LCI.

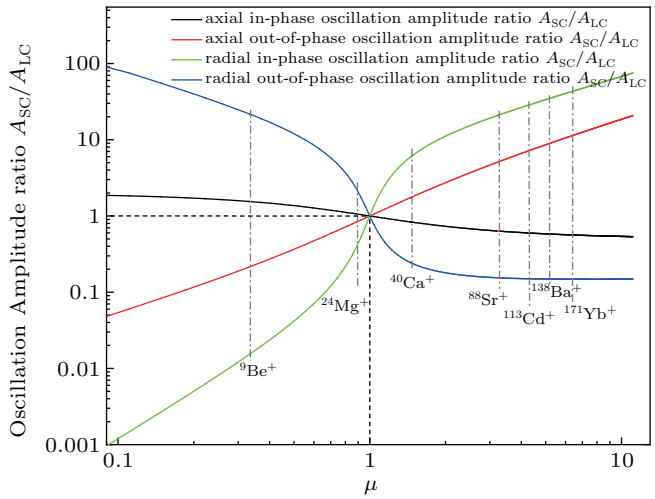


Fig. 5. Relationships between the relative resonance amplitudes of the in-phase/out-of-phase modes of an LCI–SCI pair in each dimension and their mass ratio μ.

In the $0.1 < \mu < 10$ interval, the difference between the axial (in- and out-of-phase) modes of the ion pair are significantly smaller than that between the radial modes, which indicates that the sympathetic coupling strength of the former is significantly higher than that of the latter.

The axial Coulomb interactions of an ion pair are dominated by the couplings of the in-phase mode, which is lower in frequency than the out-of-phase mode. In the in-phase mode, the vibrational amplitude of the heavier ion is slightly larger than that of the lighter ion. Therefore, the amplitude of the in-phase mode is dominated by the SCI or LCI if $\mu < 1$ or $\mu > 1$, respectively. Because the amplitude of the lighter ion is larger than that of the heavier ion in the out-of-phase mode, the amplitude of this mode is dominated by the LCI or SCI when $\mu < 1$ or $\mu > 1$, respectively. Therefore, during axial sympathetic interactions between an ion pair, the lower frequency in-phase mode of the heavier ion and the higher frequency out-of-phase mode of the lighter ion have relatively large vibrational amplitudes. The selection of an LCI with a slightly higher mass than that of the SCI is beneficial for the suppression of the amplitude of the LCI's axial in-phase mode through laser cooling, and it also indirectly tunes the amplitude of the SCI's axial in-phase mode. This effectively suppresses the vibrational amplitude of the dominant axial in-phase mode of the ion pair, thereby increasing the overall sympathetic cooling efficiency of the ion pair.

In the radial sympathetic interactions of the ion pair, the coupling of the lower frequency out-of-phase mode is slightly stronger than that of the higher frequency in-phase mode. In the out-of-phase mode, the amplitude of the heavier ion is larger than that of the lighter ion, while the reverse is true for the in-phase mode.

As a whole, the four coupling relationships of the ion pair exhibit the following behaviors: the axial in-phase modes have the strongest coupling, followed by the axial out-of-phase modes, radial out-of-phase modes, and lastly, the radial in-phase modes. The vibrational amplitudes of the heavier and lighter ions always dominate the lower and higher frequency vibrational modes, respectively. Reducing the mass mismatching in the ion pair suppresses inter-ion amplitude differences (in all vibrational modes and dimensions), improves vibrational mode coupling, and increases the sympathetic cooling rates. Conversely, excessively large mass mismatching can make simultaneous stabilization and the trapping of two different ions in a single RF field impossible, and this will also exacerbate the heating effect owing to ion micromotions. If the heating effect approaches or exceeds the (significantly worsened) sympathetic cooling effect, the sympathetic cooling efficiency of the ion pair will decrease rapidly while the equilibrium temperature rises steeply. Therefore, simultaneous trapping and sympathetic cooling of the ion pair may become impossible. If the pseudo potential well depth is maintained at reasonable values, an effective method that can be used to suppress RF heating is to reduce the radial stability parameter q of the two-ion system.[31] Because the ion pair is near the RF potential null of a linear trap, the RF heating effect for a given value of q is significantly lower than that of a 3D ion system. Therefore, the range of mass-to-charge ratio differences used for sympathetic cooling in a two-ion system is significantly larger than that used in a 3D ion system.

4.3. Optimal LCI and its coupling frequency spectra

After the SCI is determined, an optimal LCI is selected to maximize coupling and sympathetic cooling rates for the LCI–SCI pair. This ensures the fidelity of quantum-logic operations and maximizes measurement precision. In the following section, we explore the differences between ^{9}Be^{+}, ^{24}Mg^{+}, ^{40}Ca^{+}, ^{87}Sr^{+}, ^{113}Cd^{+}, ^{137}Ba^{+}, and ^{171}Yb^{+} in terms of their sympathetic interactions with ^{27}Al^{+} using secular spectra, and we then select the optimal LCI.

The Doppler cooling linewidth and cooling energy level structure of an LCI determine its Doppler cooling limit temperature, thereby affecting the sympathetic cooling efficiency

between the SCI and LCI. The Doppler cooling limit temperatures of the above mentioned seven LCIs are as follows: $T_{\min}(^{9}\mathrm{Be}^{+}) = 0.43$ mK,[32] $T_{\min}(^{24}\mathrm{Mg}^{+}) = 1.005$ mK,[33] $T_{\min}(^{40}\mathrm{Ca}^{+}) = 0.504$ mK, $T_{\min}(^{87}\mathrm{Sr}^{+}) = 0.463$ mK,[34] $T_{\min}(^{113}\mathrm{Cd}^{+}) = 1.440$ mK, $T_{\min}(^{137}\mathrm{Ba}^{+}) = 0.346$ mK, and $T_{\min}(^{171}\mathrm{Yb}^{+}) = 0.449$ mK.[35] Overall, there is no difference between these Doppler cooling limit temperatures in terms of the order of magnitude, and they are all below 2 mK. In this study, by sufficiently considering the difference between the Doppler cooling limit temperatures of different LCIs and various heating effects, the equilibrium temperatures of all the LCIs are adjusted in a unified manner to the order of 5 mK (this temperature is higher than the Doppler cooling limit temperature of each ion and is within the common equilibrium temperature range that can be realized in experiments), while focusing on the motional mode coupling effects on the sympathetic cooling efficiency. Following on from the basic conclusion, a targeted analysis is performed to examine the additional effects of the difference between the Doppler cooling limit temperatures of the main candidate ions on the conclusion.

Table 1. Numerical calculated 3D motion mode spectra $\omega_{z,r}$ and normalized mode coupling intensity $I_{z,r}$ for trapped single ion and mixed-species LCI–SCI pairs when $^{9}\mathrm{Be}^{+}$, $^{24}\mathrm{Mg}^{+}$, $^{40}\mathrm{Ca}^{+}$, $^{87}\mathrm{Sr}^{+}$, $^{113}\mathrm{Cd}^{+}$, $^{137}\mathrm{Ba}^{+}$, and $^{171}\mathrm{Yb}^{+}$ were used as the LCI for the sympathetic cooling of $^{27}\mathrm{Al}^{+}$ (the radial stability parameter of $^{27}\mathrm{Al}^{+}$ is $q_{\mathrm{Al}} = 0.215$, the pseudo potential well depth of $^{27}\mathrm{Al}^{+}$ is $D_{\mathrm{r,Al}} = 0.136$ eV).

Configuration	Motion mode	Axial		Radial	
		ω_z (kHz)	I_z	ω_r (kHz)	I_r
Single $^{40}\mathrm{Ca}^{+}$	basic mode	$\omega_{\mathrm{Ca}\text{-}z}$: 112.658	–	$\omega_{\mathrm{Ca}\text{-}r$: 174.301	–
Single $^{27}\mathrm{Al}^{+}$	basic mode	$\omega_{\mathrm{Al}\text{-}z}$: 137.315	–	$\omega_{\mathrm{Al}\text{-}r$: 268.254	–
$^{9}\mathrm{Be}^{+}$–$^{27}\mathrm{Al}^{+}$	in-phase	$\omega_{\mathrm{i},z}$: 160.697	$I_{\mathrm{i},z}$: 1.548	$\omega_{\mathrm{i},r}$: 891.912	$I_{\mathrm{i},r}$: 0.0154
	out-of-phase	$\omega_{\mathrm{o},z}$: 358.806	$I_{\mathrm{o},z}$: 0.215	$\omega_{\mathrm{o},r}$: 242.547	$I_{\mathrm{o},r}$: 21.684
$^{24}\mathrm{Mg}^{+}$–$^{27}\mathrm{Al}^{+}$	in-phase	$\omega_{\mathrm{i},z}$: 141.992	$I_{\mathrm{i},z}$: 1.060	$\omega_{\mathrm{i},r}$: 292.911	$I_{\mathrm{i},r}$: 0.403
	out-of-phase	$\omega_{\mathrm{o},z}$: 245.297	$I_{\mathrm{o},z}$: 0.839	$\omega_{\mathrm{o},r}$: 235.094	$I_{\mathrm{o},r}$: 2.208
$^{40}\mathrm{Ca}^{+}$–$^{27}\mathrm{Al}^{+}$	in-phase	$\omega_{\mathrm{i},z}$: 122.172	$I_{\mathrm{i},z}$: 0.828	$\omega_{\mathrm{i},r}$: 253.071	$I_{\mathrm{i},r}$: 6.233
	out-of-phase	$\omega_{\mathrm{o},z}$: 219.650	$I_{\mathrm{o},z}$: 1.790	$\omega_{\mathrm{o},r}$: 151.188	$I_{\mathrm{o},r}$: 0.238
$^{87}\mathrm{Sr}^{+}$–$^{27}\mathrm{Al}^{+}$	basic mode	$\omega_{\mathrm{Sr}\text{-}z}$: 76.938	–	$\omega_{\mathrm{Sr}\text{-}r$: 66.974	–
$^{113}\mathrm{Cd}^{+}$–$^{27}\mathrm{Al}^{+}$	basic mode	$\omega_{\mathrm{Cd}\text{-}z}$: 67.850	–	$\omega_{\mathrm{Cd}\text{-}r$: 47.206	–
$^{137}\mathrm{Ba}^{+}$–$^{27}\mathrm{Al}^{+}$	basic mode	$\omega_{\mathrm{Ba}\text{-}z}$: 61.388	–	$\omega_{\mathrm{Ba}\text{-}r$: 34.058	–
$^{171}\mathrm{Yb}^{+}$–$^{27}\mathrm{Al}^{+}$	basic mode	$\omega_{\mathrm{Yb}\text{-}z}$: 55.236	–	$\omega_{\mathrm{Yb}\text{-}r$: 21.274	–

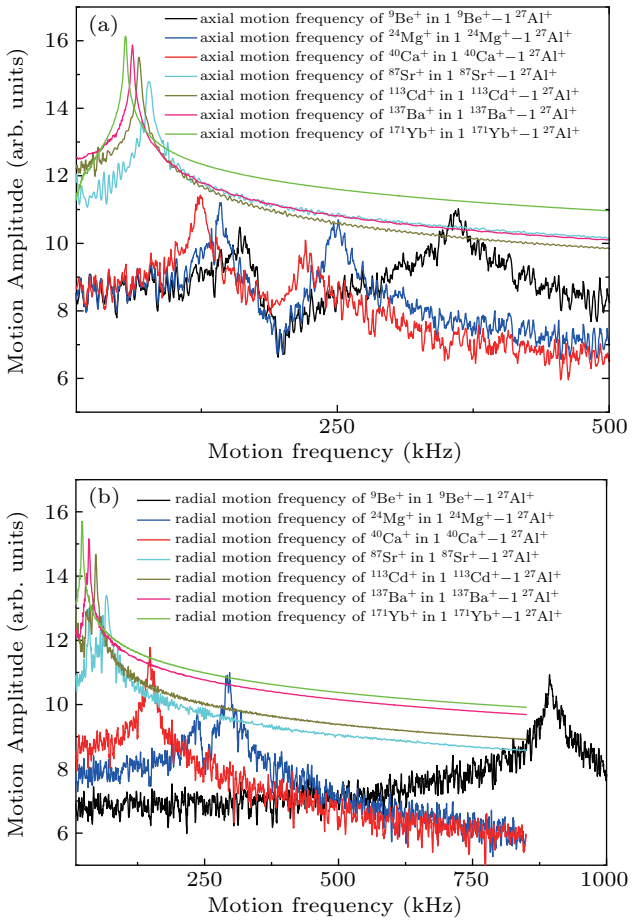


Fig. 6. (a) Axial and (b) radial secular spectra that were observed when $^{9}\mathrm{Be}^{+}$, $^{24}\mathrm{Mg}^{+}$, $^{40}\mathrm{Ca}^{+}$, $^{87}\mathrm{Sr}^{+}$, $^{113}\mathrm{Cd}^{+}$, $^{137}\mathrm{Ba}^{+}$, and $^{171}\mathrm{Yb}^{+}$ were used as the LCI for the sympathetic cooling of $^{27}\mathrm{Al}^{+}$.

As mentioned previously, the sympathetic cooling rates of an LCI–SCI ion pair are primarily determined by the coupling of their axial vibrational modes, with secondary contributions from radial mode coupling. Figure 6 shows the axial (Fig. 6(a)) and radial (Fig. 6(b)) secular spectra of the LCI in seven different SCI-LCI pairs ($^{9}\mathrm{Be}^{+}$, $^{24}\mathrm{Mg}^{+}$, $^{40}\mathrm{Ca}^{+}$, $^{87}\mathrm{Sr}^{+}$, $^{113}\mathrm{Cd}^{+}$, $^{137}\mathrm{Ba}^{+}$, and $^{171}\mathrm{Yb}^{+}$ as the LCI, with $^{27}\mathrm{Al}^{+}$ as the SCI, under the RF field: $\Omega_{\mathrm{rf}} = 3.7148$ MHz, $U_{\mathrm{rf1}} = 200$ V, $U_{\mathrm{end}} = 3.5$ V. The radial stability parameter of $^{27}\mathrm{Al}^{+}$ is $q_{\mathrm{Al}} = 0.215$, and the pseudo potential well depth of $^{27}\mathrm{Al}^{+}$ is $D_{\mathrm{r,Al}} = 0.136$ eV). Significant in- and out-of-phase modes may be observed in the axial secular spectra of $^{9}\mathrm{Be}^{+}$, $^{24}\mathrm{Mg}^{+}$, and $^{40}\mathrm{Ca}^{+}$, which is indicative of strong coupling with $^{27}\mathrm{Al}^{+}$. In the radial secular spectra, $^{24}\mathrm{Mg}^{+}$ shows significant in- and out-of-phase modes, and $^{40}\mathrm{Ca}^{+}$ exhibits a significantly stronger out-of-phase mode than in-phase mode. Be^{+} exhibits a significant in-phase mode; however, the intensity of its out-of-phase mode is negligible. $^{87}\mathrm{Sr}^{+}$, $^{113}\mathrm{Cd}^{+}$, $^{137}\mathrm{Ba}^{+}$, and $^{171}\mathrm{Yb}^{+}$ only exhibit one significant vibrational peak in their axial and radial spectra, which closely matches their theoretical secular frequency. Shown in Fig. 6, the 3D motion mode main spectra peak $\omega_{z,r}$ and normalized mode coupling intensity $I_{z,r}$

for trapped mixed-species LCI–SCI pairs are summarized and compared in Table 1. It may be assumed that $^{24}Mg^+$, ^{40}Ca, and $^9Be^+$ formed tightly coupled ion systems with $^{27}Al^+$, whereas $^{87}Sr^+$, $^{113}Cd^+$, $^{137}Ba^+$, and $^{171}Yb^+$ formed weakly coupled ion systems with large mass mismatches.

Figure 7 shows the (a) axial and (b) radial secular spectra of the (tightly coupled) $^{24}Mg^+$–$^{27}Al^+$, $^{40}Ca^+$–$^{27}Al^+$, and $^9Be^+$–$^{27}Al^+$ ion pairs (under the RF field: $\Omega_{rf} = 3.7148$ MHz, $U_{rf1} = 200$ V, $U_{end} = 3.5$ V, the radial stability parameter of $^{27}Al^+$ is $q_{Al} = 0.215$, and the pseudo potential well depth of $^{27}Al^+$ is $D_{r,Al} = 0.136$ eV). These three ion pairs exhibited in- and out-of-phase modes in all three dimensions. The matching errors between the resonance peaks of the ion pairs and their mode coupling theory-predicted in- and out-of-phase modes were generally less than 2%. In addition, the in- and out-of-phase modes of the ion pairs generally red shifted with increasing LCI mass.

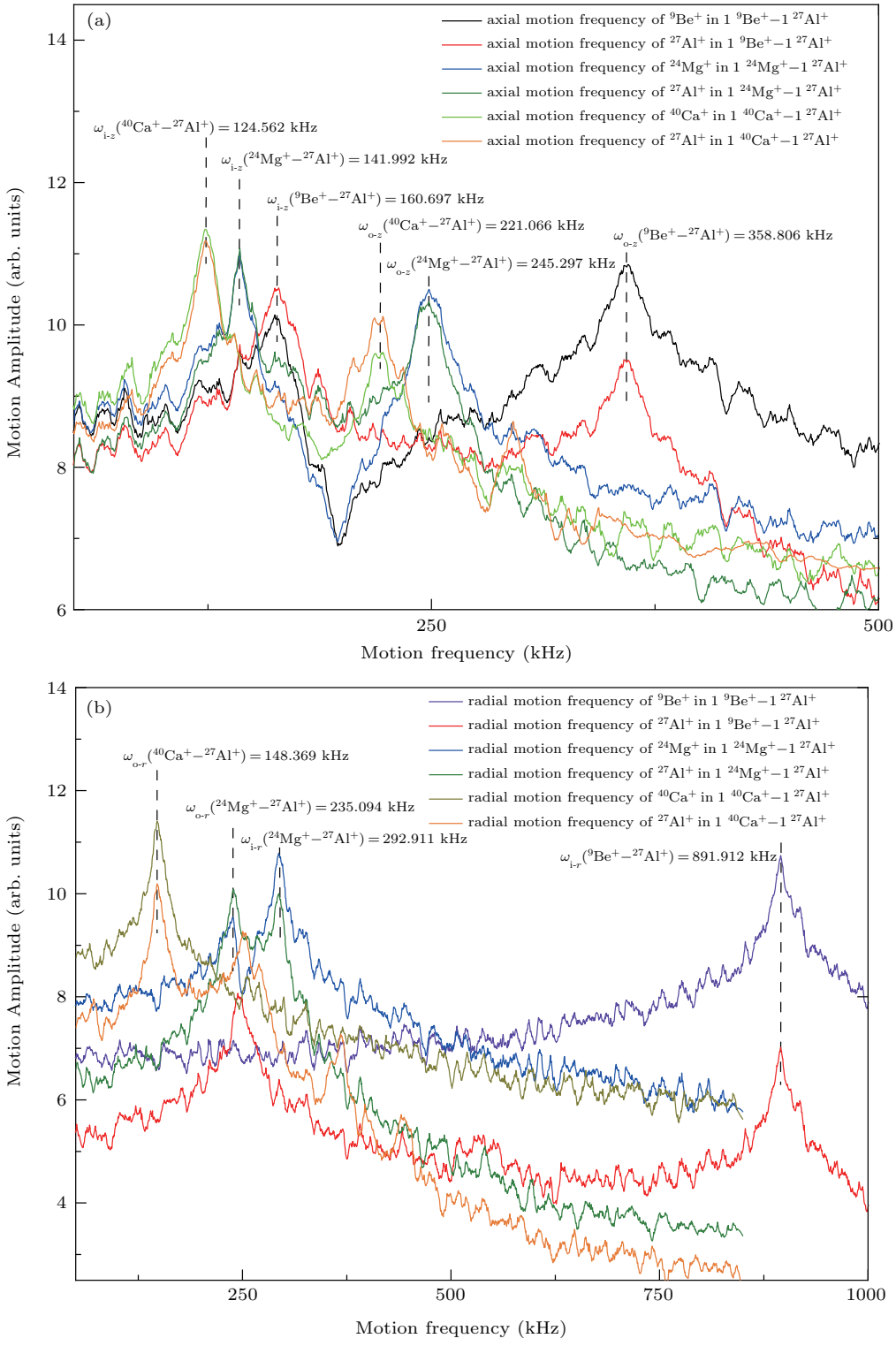


Fig. 7. (a) Axial and (b) radial motional spectra of the $^9Be^+$–$^{27}Al^+$, $^{24}Mg^+$–$^{27}Al^+$, and $^{40}Ca^+$–$^{27}Al^+$ pairs.

In the axial direction, the in-phase (out-of-phase) modes of the $^{24}Mg^+$ and $^{27}Al^+$ in the $^{24}Mg^+$–$^{27}Al^+$ pair are relatively similar to each other in amplitude, which is indicative of strong coupling. The ions in the $^{40}Ca^+$–$^{27}Al^+$ pair are strongly coupled through their in-phase vibrational modes; however, the out-of-phase mode of $^{27}Al^+$ is slightly stronger than that of $^{40}Ca^+$, which is indicative of weaker coupling. In the $^{9}Be^+$–$^{27}Al^+$ pair, the in-phase mode of $^{27}Al^+$ is slightly stronger than that of $^{9}Be^+$, whereas its out-of-phase mode is significantly weaker, and the overall coupling of the $^{9}Be^+$–$^{27}Al^+$ pair is considerably weaker than that of the $^{40}Ca^+$–$^{27}Al^+$ pair. In the radial direction, the in- and out-of-phase modes of the ions in the $^{24}Mg^+$–$^{27}Al^+$ pair are both strongly coupled. The $^{40}Ca^+$–$^{27}Al^+$ pair is strongly coupled in the radial out-of-phase mode, but weakly coupled in the radial in-phase mode. In the $^{9}Be^+$–$^{27}Al^+$ pair, the in-phase mode of $^{27}Al^+$ is significantly weaker than that of $^{9}Be^+$, which is indicative of weak coupling. The out-of-phase mode of $^{27}Al^+$ is stronger than that of $^{9}Be^+$ by several orders of magnitude, indicating that their coupling is negligible.

Based on the results above, it may be concluded that the $^{24}Mg^+$–$^{27}Al^+$ pair has the strongest sympathetic interactions, in both the axial and radial directions. The $^{40}Ca^+$–$^{27}Al^+$ pair exhibits the second strongest interactions, and the $^{9}Be^+$–$^{27}Al^+$ pair has the weakest sympathetic interactions. However, the Doppler cooling limit temperature of $^{40}Ca^+$ ($T_{\min}(^{40}Ca^+) = 0.504$ mK) is comparable to that of $^{9}Be^+$ ($T_{\min}(^{9}Be^+) = 0.43$ mK) but lower than approximately half of that of $^{24}Mg^+$ ($T_{\min}(^{24}Mg^+) = 1.005$ mK). Furthermore, laser cooling systems for $^{40}Ca^+$ are more reliable than those for $^{24}Mg^+$ and $^{9}Be^+$ (both the 397 nm and 866 nm cooling lasers for $^{40}Ca^+$ can be directly generated from an external-cavity semiconductor laser, whereas the 280 nm cooling laser for $^{24}Mg^+$ needs to be indirectly generated by frequency multiplication and the 313 nm cooling laser for $^{9}Be^+$ needs to be indirectly generated by frequency multiplication and combination). Therefore, the $^{40}Ca^+$–$^{27}Al^+$ pair is probably the best ion pair for sympathetic cooling and logic operations and has particularly more notable comprehensive advantages in engineering applications such as the development of compact, transportable $^{27}Al^+$ optical clocks with high environmental adaptabilities.

5. Conclusion

In this study, we have investigated the motional mode coupling of sympathetically cooled mixed-ion crystals by quantifying the 3D secular spectra of trapped ions. The 3D resonance peaks of the $^{40}Ca^+$–$^{27}Al^+$ pair obtained by using this method were in good agreement with the in- and out-of-phase modes predicted by the mode coupling theory for a pair of ions in equilibrium. The sympathetic cooling efficiency of the $^{40}Ca^+$–$^{27}Al^+$ pair is primarily determined by the coupling of the ion axial modes. The axial in-phase mode was the most strongly coupled mode, followed by the axial out-of-phase mode, radial out-of-phase mode, and lastly, the radial in-phase mode. The vibrational amplitudes of the heavier and lighter ions dominate the lower and higher frequency modes, respectively. Decreasing the mass mismatching in an ion pair improves their coupling in all dimensions, thereby improving the sympathetic cooling rates. $^{87}Sr^+$, $^{113}Cd^+$, $^{137}Ba^+$, and $^{171}Yb^+$ formed weakly coupled, highly mismatched ion systems with $^{27}Al^+$, whereas $^{24}Mg^+$, $^{40}Ca^+$, and $^{9}Be^+$ formed tightly coupled ion systems with $^{27}Al^+$. Compared with the $^{24}Mg^+$–$^{27}Al^+$ pair and $^{9}Be^+$–$^{27}Al^+$ pair, laser cooling systems for the $^{40}Ca^+$–$^{27}Al^+$ pair are more reliable, and the latter has a minimum cooling temperature as low as 0.5 mK. Therefore, the $^{40}Ca^+$–$^{27}Al^+$ pair is probably the best overall pairing for sympathetic cooling and logic operations and has particularly more notable comprehensive advantages in the development of highreliability, compact, transportable $^{27}Al^+$ optical clocks. Highly charged ion (HCI) optical clocks and nuclear optical clocks are new interests in the fields of research in recent years. These ions exhibit better linewidths and environmental immunity compared to the outer-layer electron transition properties of conventional singly charged ions and are currently pinning great hopes on sympathetic cooling and quantum-logic measurements to achieve optical clock applications. The high-charge properties of HCIs often result in extremely low mass-to-charge ratios (e.g., Ar^{13+}). $^{9}Be^+$ is currently the best match for HCIs in terms of the sympathetic cooling efficiency. For the HCI-LCI pair, it is necessary to further focus on the effects of the strong Coulomb interactions between the ions caused by the high-charge properties on ion cooling. The amplitude of an HCI's excess micromotion is positively correlated with its charge, Q, and they are much more sensitive to external perturbations than those of SCI systems. The trapping lifetime of HCIs may be greatly shortened by collision-induced charge transfer, which results in issues such as the creation of down-charged HCIs. Therefore, more stringent requirements are introduced for the level of vacuum and assembly accuracy of ion traps, the suppress the heating effects of random electronic thermal noise and micromotion, efficient ion trapping from high to low energy, and external-state high-fidelity coupling over long distances. As a candidate ion for nuclear optical clocks, $^{229}Th^{3+}$ garners the most attention.[36,37] Sr^+ may be a relatively suitable LCI for sympathetic cooling of $^{229}Th^{3+}$ due to the following main reasons: Sr^+ and $^{229}Th^{3+}$ have similar mass-to-charge ratios, which can facilitate motional mode coupling. The cooling lasers for Sr^+ are relatively mature (both the 422 nm and 1092 nm lasers can be generated directly from a semiconductor laser), and Sr^+ has a minimum Doppler cooling limit temperature as low as 0.463 mK. In addition, Sr^+ itself has a relatively good optical clock transition reference. As a result, $^{229}Th^{3+}$ and Sr^+ can be evaluated by measurement comparisons in the same external field environment. The Sr^+–$^{229}Th^{3+}$ pair has

notable advantages in measuring the time-varying characteristics of fundamental physical constants. The outcomes presented in this study will contribute to the development of high-fidelity quantum-logic techniques based on the multiple resonance modes, efficient sympathetic cooling for highly charged ions, and the construction of more precise atomic clocks.

References

[1] Safronova M S, Budker D, DeMille D, Kimball D F J, Derevianko A and Clark C W 2018 *Rev. Mod. Phys.* **90** 025008

[2] Brewer S M, Chen J S, Hankin A M, Clements E R, Chou C W, Wineland D J, Hume D B and Leibrandt D R 2019 *Phys. Rev. Lett.* **123** 033201

[3] Von der Wense L, Seiferle B, Laatiaoui M, Neumayr J B, Maier H J, Wirth H F, Mokry C, Runke J, Eberhardt K, Düllmann C E and Trautmann N G 2016 *Nature* **533** 47

[4] Seiferle B, Von der Wense L, Bilous P V, Amersdorffer I, Lemell C, Libisch F, Stellmer S, Schumm T, Düllmann C E, Pálffy A and Thirolf P G 2019 *Nature* **573** 243

[5] Dzuba V A, Flambaum V V and Katori H 2015 *Phys. Rev. A* **91** 022119

[6] Yudin V I, Taichenachev A V and Derevianko A 2014 *Phys. Rev. Lett.* **113** 233003

[7] Derevianko A, Dzuba V A and Flambaum V V 2012 *Phys. Rev. Lett.* **109** 180801

[8] Chou C W, Hume D B, Rosenband T and Wineland D J 2010 *Science* **329** 1630

[9] Chen J S, Brewer S M, Chou C W, Wineland D J, Leibrandt D R and Hume D B 2017 *Phys. Rev. Lett.* **118** 053002

[10] Walz J, Ross S B, Zimmermann C, Ricci L, Prevedelli M and Hansch T W 1995 *Phys. Rev. Lett.* **75** 3257

[11] Germann M, Tong X and Willitsch S 2014 *Nat. Phys.* **10** 820

[12] Raghunandan M, Wolf F, Ospelkaus C, Schmidt P O and Weimer H 2020 *Science Adv.* **6** eaaw9268

[13] Monroe C, Meekhof D M, King B E, Itano W M and Wineland D J 1995 *Phys. Rev. Lett.* **75** 4714

[14] Häffner H, Hänsel W, Roos C F, Benhelm J, Chwalla M, Körber T, Rapol U D, Riebe M, Schmidt P O, Becher C and Gühne O 2005 *Nature* **438** 643

[15] Riebe M, Monz T, Kim K, Villar A S, Schindler P, Chwalla M, Henrich M and Blatt R 2008 *Nat. Phys.* **4** 839

[16] Home J P, Hanneke D, Jost J D, Amini J M, Leibfried D and Wineland D J 2009 *Science* **325** 1227

[17] Wan Y, Gebert F, Wolf F and Schmidt P O 2015 *Phys. Rev. A* **91** 043425

[18] Inlek I V, Crocker C, Lichtman M, Sosnova K, and Monroe C 2017 *Phys. Rev. Lett.* **118** 250502

[19] Zhang J, Deng K, Luo J, Lu Z H 2017 *Chin. Phys. Lett.* **34** 050601

[20] Du L J, Chen T, Song H F, Chen S L, Li H X, Huang Y, Tong X, Guan H and Gao K L 2015 *Chin. Phys. B* **24** 083702

[21] Du L J, Song H F, Li H X, Chen S L, Chen T, Sun H Y, Huang Y, Tong X, Guan H and Gao K L 2015 *Chin. Phys. B* **24** 113703

[22] James D F V 1998 *Appl. Phys. B* **66** 181

[23] Wineland D J, Monroe C, Itano W M, Leibfried D, King B E and Meekhof D M 1998 *J. Res. Natl. Inst. Stand. Technol.* **103** 259

[24] Kielpinski D, King B E, Myatt C J, Sackett C A, Turchette Q A, Itano W M, Monroe C, Wineland D J and Zurek W H 2000 *Phys. Rev. A* **61** 032310

[25] Wübbena J B, Amairi S, Mandel O and Schmidt P O 2012 *Phys. Rev. A* **85** 043412

[26] Bruzewicz C D, McConnell R, Stuart J, Sage J M and Chiaverini J 2019 *npj Quantum Inf* **5** 1

[27] Verlet L 1967 *Phys. Rev.* **159** 98

[28] Verlet L 1968 *Phys. Rev.* **165** 201

[29] Zhang M Q and Skeel R D 1995 *J. Comput. Chem.* **16** 365

[30] Berkeland D J, Miller J D, Bergquist J C, Itano W M and Wineland D J 1998 *J. Appl. Phys.* **83** 5025

[31] Paul W, Osberghaus O and Fischer E 1958 *Forschungsberichte des Wirtschafts und Verkehrsministeriums Nordrhein-Westfalen* 415

[32] Brian C S, Joseph W B, and John J B 2014 *Phys. Rev. A* **89** 033408

[33] Knünz S, Herrmann M, Batteiger V, Saathoff G, Hänsch T W, Vahala K, and Udem T 2010 *Phys. Rev. Lett.* **105** 013004

[34] Removille S, Dubessy R, Dubost B, Glorieux Q, Coudreau T, Guibal S, Likforman J P and Guidon L 2009 *J. Phys. B* **42** 154014

[35] Mulholland S, Klein H A, Barwood G P, Donnellan S, Gentle D, Huang G, Walsh G, Baird P E G and Gill P 2019 *Appl. Phys. B* **125** 198

[36] Campbell C J, Radnaev A G, Kuzmich A, Dzuba V A, Flambaum V V and Derevianko A 2012 *Phys. Rev. Lett.* **108** 120802

[37] Seiferle B, Wense L V D, Bilous P V, Amersdorffer I, Lemell C, Libisch F, Stellmer S, Schumm T, Christoph E D, Pálffy A and Thirolf P G 2019 *Nature* **573** 243